DELIVERY OF MINOXIDIL AND VALPROIC ACID FOR THE TREATMENT OF ANDROGENETIC ALOPECIA UNDER ELECTRICAL STIMULATION

Peixin Li[a,b], Zhenyu Wu[a,b], Nan Chen[a,b], Khurshidabonu I. Burkhonova[c], Khaydar E. Yunusov[c], Yanfang Sun[d], Guohua Jiang[a,b,e,*]

[a] *School of Materials Science and Engineering, Zhejiang Sci-Tech University, Hangzhou, 310018, China*
[b] *International Scientific and Technological Cooperation Base of Intelligent Biomaterials and Functional Fibers, Hangzhou, 310018, China*
[c] *Institute of Polymer Chemistry and Physics, Uzbekistan Academy of Sciences, Tashkent, 100128, Uzbekistan*
[d] *College of Life Sciences and Medicine, Zhejiang Sci-Tech University, Hangzhou, China*
[e] *Zhejiang-Mauritius Joint Research Center for Biomaterials and Tissue Engineering, Zhejiang Sci-Tech University, Hangzhou 310018, P. R. China*

E-mail:ghjiang_cn@zstu.edu.cn (G. Jiang)

Abstract.

Androgenetic alopecia (AGA) is a worldwide and cross-gender disease that is usually treated by continuous administration of minoxidil (MXD). However, MXD can only slow hair loss and may cause hirsutism due to its low absorption effect. In this work, an MXD-loaded microneedles (MNs) system with the assistance of valproic acid (VPA) was developed to treat AGA under electrical stimulation (ES). The matrix of MXD-loaded MNs consisted of carboxymethylcellulose (CMC), hyaluronic acid (HA) and polyvinylpyrrolidone (PVP). The microneedles could create microchannels after their insertion into the skin, and the transdermal efficiency of the loaded MXD could be enhanced under ES. *In vivo* results in C57BL/6J rats showed that the as-fabricated MXD-loaded MNs promoted hair growth via transdermal delivery of minoxidil and valproic acid under ES by upregulating Wnt/beta-catenin in VPA, promoting the secretion of vascular endothelial growth factor (VEGF) and activating hair follicle stem cells.

Keywords: Minoxidil, valproic acid, androgenetic alopecia, electrical stimulation, hair regeneration

DELIVERY OF MINOXIDIL AND VALPROIC ACID FOR THE TREATMENT OF ANDROGENETIC ALOPECIA UNDER ELECTRICAL STIMULATION

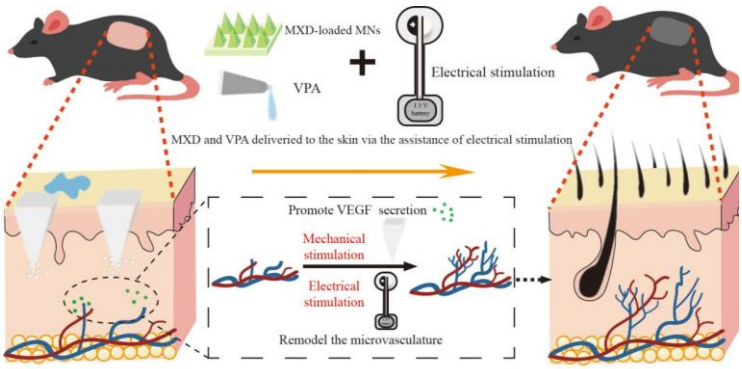

1. Introduction

Androgenetic alopecia (AGA) is the predominant form of hair loss and primarily affects young and middle-aged males [1-3]. It is characterized by a greater rate of hair loss than hair growth [4-7]. The increasing number of individuals experiencing hair loss, along with the growing demand for hair restoration, indicates a promising market for hair regrowth [8-11]. Current treatment strategies for AGA include topical minoxidil (MXD), oral finasteride (FIN), and hair follicle (HF) transplantation [12-15]. However, these treatments have significant limitations. For instance, minoxidil requires twice-daily application, which can be inconvenient, and may cause scalp irritation. Finasteride, on the other hand, is associated with systemic side effects such as decreased libido, erectile dysfunction, and depression. Moreover, both medications require continuous use to maintain their benefits [16-18]. Hair follicle transplantation as a surgical procedure has its own set of risks, such as lower availability of viable hair follicles and related costs [19, 20].

Although MXD has demonstrated positive outcomes in AGA treatment, it may be more susceptible to cutaneous side effects and hirsutism [21-23]. Due to the skin barrier, the actual absorption of MXD by hair follicle cells is still limited [24-26]. Valproic acid (VPA) is an FDA-approved anticonvulsant drug that effectively stimulates HF regrowth by upregulating Wnt/β-catenin. Currently, the only available route for administering VPA to induce hair regrowth is the topical delivery of solvent-based VPA (topical VPA). However, long-term administration of organic solvent-based therapeutics may irreversibly damage human health [27].

AGA treatment mediated by MNs is a painless method for drug transdermal delivery, offering the advantages of ease of administration, minimal tissue trauma, and cost-effectiveness [30-32]. It effectively overcomes the barrier posed by the stratum corneum, facilitating drug penetration into both the epidermis and dermis [33, 34]. The current trend in clinical research and practical applications involves the gradual introduction of nonpharmacological therapies, such as thermal stimulation, electrical stimulation, and photostimulation [35-38]. These therapies typically utilize alternating electric fields (EFs) within the frequency range of 0.1-10 V/cm^2 and <15 Hz, which have minimal tissue damage effects [39, 40]. The electrical stimulation effect is believed to concurrently regulate the secretion of growth factors, such as vascular endothelial growth factor (VEGF), which facilitates the proliferation of hair follicles (HFs), extends the anagen phase, and ultimately stimulates hair regrowth [41, 42]. The current *in vitro* therapeutic equipment, however, remains bulky and impractical for daily treatment [43]. Moreover, the efficacy of electrical stimulation alone in promoting hair regeneration is relatively insignificant.

Herein, a system incorporating MXD-loaded MNs and VPA was designed for the treatment of AGA with the assistance of electrical stimulation. Using the inherent function of MXD-loaded MNs to overcome the skin barrier, the encapsulated MXD and VPA were physically penetrated and implanted inside the skin. Carboxymethyl cellulose (CMC), hyaluronic acid (HA) and polyvinylpyrrolidone (PVP) were selected as the MN matrices due to their biocompatibility, biodegradability, and rapid dissolution in the skin's extracellular fluid, leading to improved drug permeation. Subsequently, the hair growth-promoting effects of MXD-loaded MNs, VPA and electrical stimulation were evaluated in C57BL/6J rats (Fig. S1).

2. Experimental section

2.1 Materials

Minoxidil (MXD, >98.0%), valproic acid (VPA, >98.0%), carboxymethyl cellulose sodium (CMC, 1500-3100 mPa·s), hyaluronic acid (HA, 95%), polyvinylpyrrolidone (PVP, K30), phosphate-buffered saline (PBS), acetate (36%), TWEEN® 80 and ethanol (>99.5%) were obtained from Aladdin Chemical Reagent Co., Ltd. (Shanghai, China). Testosterone was purchased from Beyotime Biotechnology (Shanghai, China). Dulbecco's modified Eagle's medium (DMEM) was obtained from Procell Life Science & Technology Co., Ltd. (Shanghai, China).

2.2 Preparation of MXD-loaded MNs

The preparation of blank MNs followed procedures described in previous work [44, 45]. First, solution A [CMC (0.3 g), HA (0.15 g) and PVP (0.9 g)] was dissolved in deionized water (15.3 mL) and stirred for 24 h. The solution was then prepared and cast onto the surface of polydimethylsiloxane (PDMS) molds. After that, the residual solution was scraped off from the PDMS template by a medical spoon. The blank MNs were gently peeled off from the PDMS molds and stored before use after drying for 24 h. For the preparation of the MXD-loaded MNs, MXD (0.3 g) was dissolved in solution A (15 g) and stirred for 24 h, after which the MXD-loaded MN patches were prepared as described above. The morphologies of the as-obtained MN patches were characterized by field emission scanning electron microscopy (FE-SEM, Vltra55, Zeiss) at an extra high tension of 5 kV and a digital microscope (DTM, BST500xUSB).

2.3 Mechanical strength and skin penetration tests

The mechanical properties of the MNs were measured by a universal material testing machine (UTM, WDW-02). The MN patches were placed on the pallet of the testing machine, and the force was continuously monitored when the top plate compressed the needles at a constant speed. The force–displacement curve was recorded. To assess *in vitro* skin penetration, MN patches loaded with rhodamine R6G (R6G-MNs) were applied to isolated rat skin for 5 min. The skin samples were immediately embedded in OCT compounds. The samples were then frozen and sectioned using a cryotome (CryostarNX50, Thermo, USA) for histological analysis. Hematoxylin and eosin (H&E) staining was conducted on the sections to visualize tissue morphology. Following H&E staining, the sections were examined under a bright-field light microscope (TS2-S-SM, Nikon, Japan).

2.4 Drug release *in vitro*

Transdermal tests were performed using the Franz diffusion cell method. Rat skin was sliced and glued to the diffusion pool with PBS containing 30% ethanol as the receiving medium. The effective transdermal area was 2 $cm^{2,}$ and the receiving cell volume was 15 mL. Freshly prepared mouse skin was inserted with an MXD-loaded MN patch and coated with 0.4 mL of VPA, which was affixed to the receiving chamber of the Franz diffusion cell. At predetermined time intervals, 1.5 mL samples were taken from the receiving cell and prompt-

ly replaced with an equal volume of the same receiving medium (PBS + 30% ethanol). The total amount of MXD released from the patch was determined using a UV–Vis spectrophotometer.

2.5 Cytotoxicity tests *in vitro* and androgenetic alopecia management *in vivo*

The cytotoxicity of the MXD-loaded MNs was tested by culturing L929 cells using MTT analysis. The hair regeneration capabilities of MXD-loaded MNs with or without electrical stimulation were evaluated in male C57BL/6 rats (6 weeks old, Moslet Biotechnology Co., Ltd., Hangzhou, China) following a previously reported method [46] with slight modifications. All the animal procedures were approved by the Animal Ethics Committee of Zhejiang Sci-Tech University (No: 20240109-10) and Moslet Biotechnology Co., Ltd. (No: MSLT-2023-0022). A 4 cm^2 area (2 cm × 2 cm) of hair from the dorsal portion of the hair of 7-week-old mice in the telogen phase was gently shaved with an electric hair clipper and depilated with hair-removing cream. The mice were randomly divided into 6 groups (Table S1): G1 (Model group: AGA mice without treatment), G2 (Control group: AGA mice treated with MXD-loaded MNs), G3 (Positive 10 min group: treated with MXD-loaded MNs and positive electrical stimulation for 10 min), G4 (Positive 60 min group: treated with MXD-loaded MNs and positive electrical stimulation for 60 min), G5 (Negative 10 min group: treated with MXD-loaded MNs and negative electrical stimulation for 10 min), and G6 (Negative 60 min group: treated with MXD-loaded MNs and negative electrical stimulation for 60 min). MXD-loaded MNs were applied to the skin to create microchannels before spreading VPA and applying electrical stimulation. Digital pictures of the skin and hair were taken at defined intervals. The diameter and density of the regrown hair were measured with the assistance of a Firefly triscope DE337T (Belmont, USA) on day 21 postdeposition.

2.6 Histology and immunohistochemistry analysis

Hematoxylin and eosin (H&E) staining was performed for histological examination to assess hair growth in AGA C67BL/6J mice. Inflammation at hair regrowth was evaluated by the interleukin 6 (IL-6) ELISA Kit. The level of vascular endothelial growth factor (VEGF) in the hair regrowth area was determined by a VEGF ELISA kit.

2.7 Statistical analysis

The statistical analysis was performed using the statistical software GraphPad Prism 7. A p value < 0.05 was considered to indicate statistical significance. $*P < 0.05$, $**P < 0.01$, $***P < 0.001$, $****P < 0.0001$.

3. Results and discussion

3.1 Synthesis and characterization of CPH and MXD@CPH

The as-fabricated MNs were arranged in a 30 × 30 array on a 20 × 20 mm patch (Fig. 1a). The as-fabricated MXD-loaded MNs exhibit a conical shape with a height of 550 μm (Fig. 1b), coupled with an intact and uniform morphology. The mechanical properties of MXD-loaded MNs are a critical factor in achieving their successful insertion into the skin [47-49]. As shown in Fig. 1c, an axial compressive load is applied to the MN patch, and the force–displacement curves are recorded against the compressive displacement. The compressive force–displacement diagram shows smooth curves without fracture within the displacement range of 0–800 μm. The compressive forces measured for the MNs were more than 0.48 and 0.50 N/needle for those without and with MXD loading, respectively, at a displacement of 400 μm. This indicates that the insertion force is sufficient to penetrate the skin, as it exceeds the minimum required force.

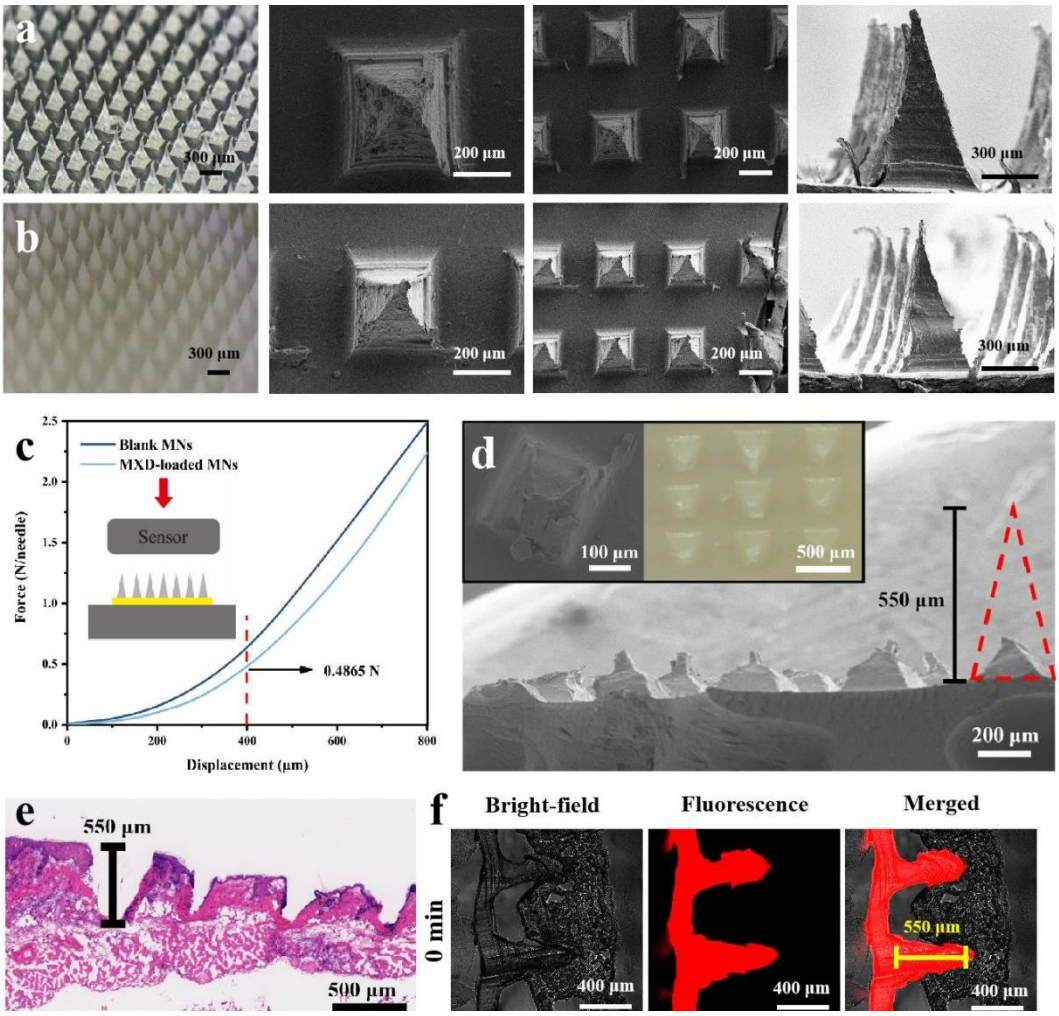

Figure 1 Bright-field microscopy image and SEM image of blank (a) and MXD-loaded MNs (b), force–displacement curves of blank and MXD-loaded MNs (c), SEM image of MXD-loaded MNs after insertion into skin (d, insets show the magnific SEM and bright-field microscopy images of MNs), H&E staining image of skin pierced by MNs (e) and laser confocal images (f) of R6G-loaded MNs after piercing into the isolated rat skin.

After insertion into the skin, the tips of the needles are broken, and most of them remain on the skin (Fig. 1d). R6G, a model red dye, is used to assist in observing the penetration performance of MNs for porcine skin. As anticipated, the R6G-loaded MNs can penetrate porcine skin. Hematoxylin-eosin (H&E)-stained histological section images showed that the MNs could successfully puncture the stratum corneum of the skin and leave microchannels on the surface of the skin. The depth of these microchannels is ~ 200-550 μm (Fig. 1e). The laser confocal images show a red area with a microneedle shape after piercing the patches into the skin, indicating successful insertion into the skin (Fig. 1f).

3.2 Drug release and cytotoxicity *in vitro*

To simulate drug delivery *in vivo*, a modified Franz diffusion cell (Fig. 2a) and positive/negative electrode (Fig. 2b) were used to measure drug delivery efficiency via a transdermal delivery route (Table S2). As shown in Fig. 2c and 2d, the cumulative drug release rates of MXD and VPA were ~79.09% and ~69.96%, respectively, with positive electrical stimulation for 120 min. In contrast, the cumulative drug release rates were ~74.96% and ~64.92%, respectively, with negative electrical stimulation for 120 min. This may be related

to the fact that negative electrical stimulation accelerates the recovery of the microtrauma caused by MNs, and the rapid recovery of the microchannels may affect drug delivery [39, 41]. However, the cumulative drug release of MXD and VPA was less than ~60% and ~10%, respectively, after 120 min without electrical stimulation. These results indicate that electrical stimulation can accelerate the drug release rate and significantly improve the transdermal efficiency of drugs by regulating the intradermal environment. Positive electrical stimulation is the best method for drug transdermal penetration.

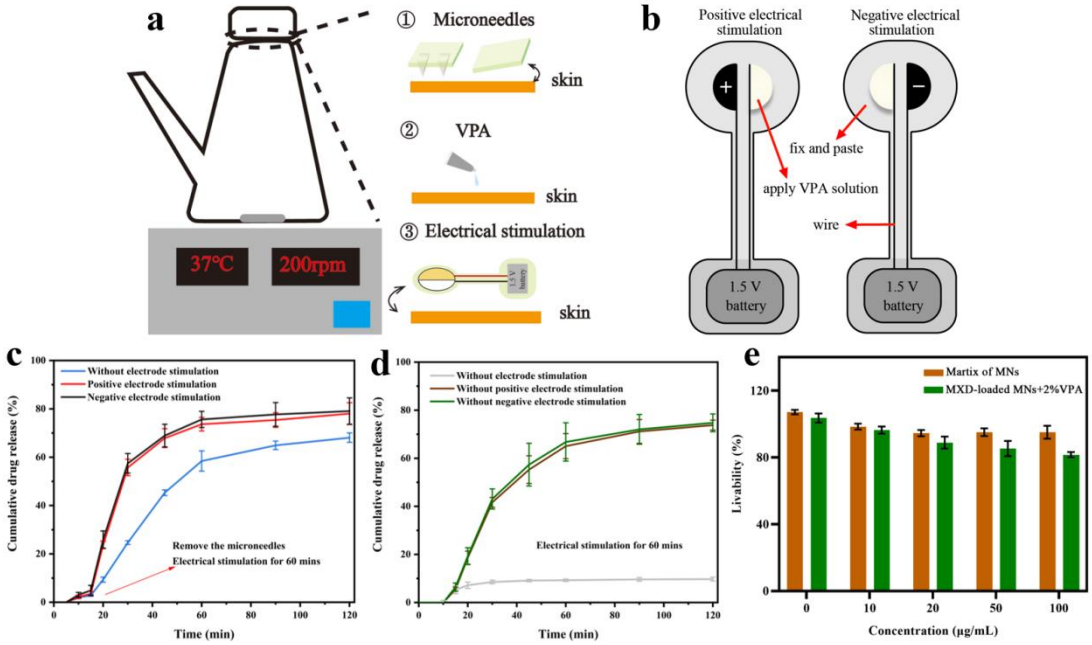

Figure 2 Schematic illustration of the Franz diffusion cell for drug release *in vitro* (a) and electrode structure of positive/negative electrical stimulation (b), the release profiles of MXD (c) and VPA (d) by a Franz diffusion cell *in vitro* under different electrical stimuli, and cell viability plots for blank and MXD-loaded MNs against L929 cells (e).

The effect of MNs on the viability of L929 cells was assessed by MTT assay. Fig. 2e shows the viability of L929 cells after co-culture for 24 h with different concentrations of MN leachate (20 μL/hole) obtained by soaking the MNs in DMEM for 24 h. The viability was greater than 80% even when the leachate concentration increased to 100 μg/mL, indicating the cytocompatibility of CMC with HA. The survival of cells loaded with MXD-loaded MNs was also assessed by MTT analysis. The viability was more than 80% for concentrations ranging from 0 to 100 μg/mL, implying negligible effects after loading MXD into the MNs.

3.3 Hair regeneration evaluation

To evaluate the efficacy of MXD-loaded MNs and electrical stimulation on hair regeneration in C57BL/6 mice, an AGA model was established by topically coating 0.5% testosterone to the dorsal depilated area of the mice for 20 days at a dose of 5 mg/kg (Fig. 3a) [50]. Different administration strategies were used on days 3, 9, and 15. Representative pictures of mice on days 0, 5, 10, and 20 during the treatment period were recorded and are shown in Fig. 3b. There was almost no hair growth within 20 days in the model group due to the inhibition of hair HF cells in the resting period by testosterone, indicating the successful establishment of the AGA mouse model. In the control group (G2: AGA mice treated with MXD-loaded MNs and VPA), HF cells began to appear in the anagen phase after 5 days. Skin darkening com-

menced on day 10 after hair removal, and noticeable hair regrowth was observed on day 20. The dorsal skin of the mice in the model group remained pink after day 10, indicating that the HFs remained in the telogen phase. This result also suggested the successful establishment of the testosterone-induced AGA model. In contrast, obvious hair regrowth can be found in the dorsal skin of mice treated with MXD-loaded MNs, VPA, and positive electrical stimulation for 10 days (G3 and G4 groups), indicating the effectiveness of hair regeneration. In addition, dorsal skin that transformed from pink to black with greater density was observed on days 15 and 20, with longer positive electrical stimulation times per treatment. Compared to those in the positive electrical stimulation groups, hair regrowth was also found in the dorsal skin of mice in the G5 and G6 groups after 10 days of negative electrical stimulation. Greater regenerated hair coverage in the G6 group than in the G5 group was observed with longer durations of negative electrical stimulation. However, the regenerated hair coverage in the G5 and G6 groups with negative electrical stimulation was slightly lower than that in the G3 and G4 groups with positive electrical stimulation even with decreased electrical stimulation frequency.

Furthermore, hair-covered areas on the dorsal surface of mice in the G1-G6 groups were evaluated for the quality of regenerated hair. As shown in Fig. 3c, 10 days after administration, the regenerated hair coverage in G2-G6 was ~25% of the dorsal depilated area. However, hair growth became faster and denser in the G3-G6 groups after 10 days of electrical stimulation. This indicates that electrical stimulation favors hair regeneration. However, the hair coverage area in the G5 and G6 groups was relatively lower than that in the G3 and G4 groups, and a lower electrical stimulation frequency led to a lower hair coverage area (Fig. 3d). These results indicate that longer positive electrical stimulation has a better synergistic effect on hair regeneration.

Fig. 3e shows the hair density under different treatment strategies after 20 days of treatment. There were only ~2,000 shafts/cm^2 for the G2 group with only the administration of MXD-loaded MNs and VPA. The MXD and VPA can only slowly diffuse into the skin through the microchannels formed by MNs. However, under electrical stimulation, the hair density can increase to more than ~3,000 shafts/cm^2 in the same administration period. This indicates that electrical stimulation is favorable for the transdermal delivery of MXD and VPA into skin tissue due to the electrostatic repulsion between electrical stimulation and drugs.

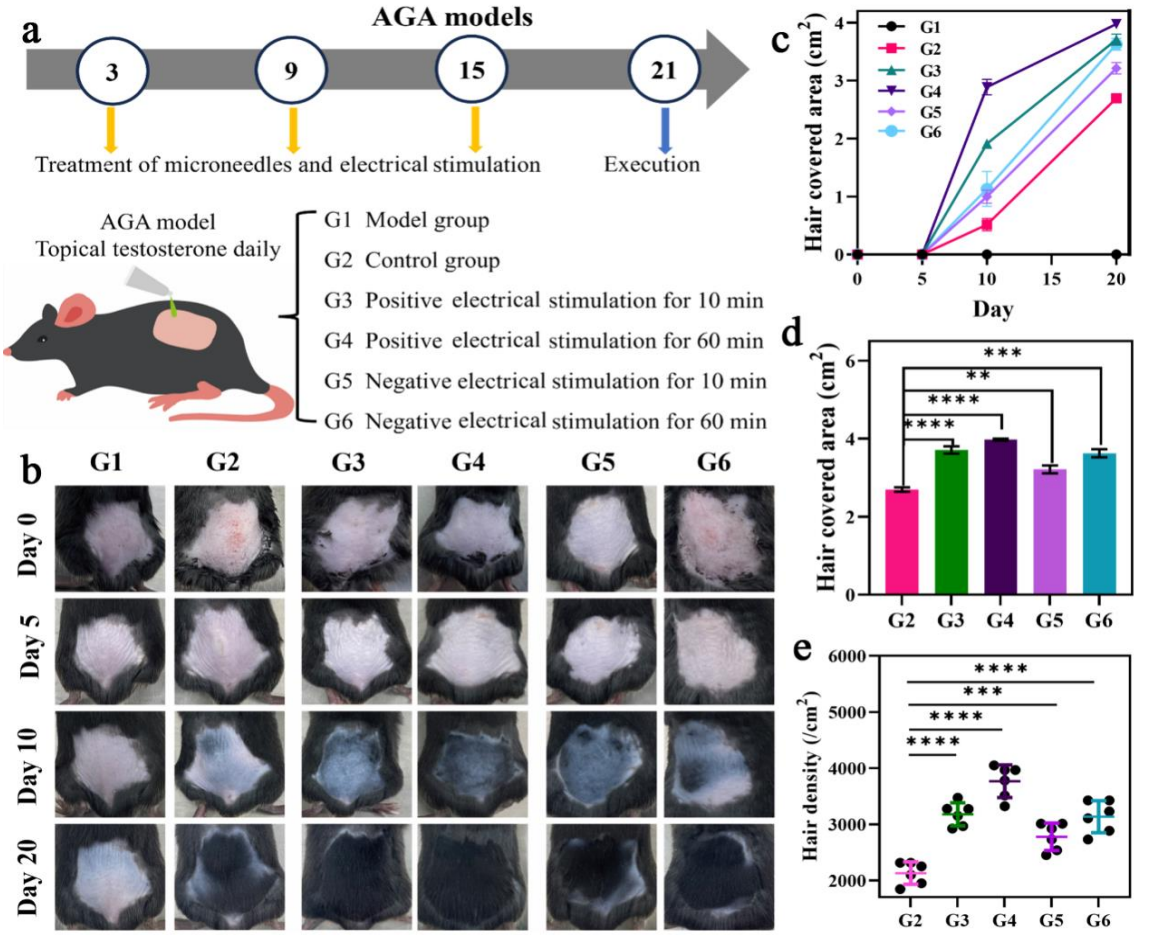

Figure 3 Schematic for the establishment of and therapeutic strategies for AGA mice (a), representative images of hair regeneration *in vivo* (b), hair-covered areas on the backs of mice in the G1-G6 groups (c), and comparison of the hair-covered areas (d) and hair density (e) in the G2-G6 groups after administration for 20 days.

The effect of MXD, VPA, and electrical stimulation on hair regrowth quality was evaluated by quantifying the length (mm) and diameter (μm) of the dorsal skin area. Fig. 4a shows the average hair length after 12 days of administration. The average hair length of the G2 group was only ~2.80 mm, which was the shortest among the G2-G6 groups. The average hair length of G4 was 5.90 mm, which was the longest among all the tested groups. This indicates that the synergistic effect of MXD-loaded MNs, VPA and longer electrical stimulation can produce the greatest effect on hair regeneration. In addition, the average hair diameter of the G2 group was 18.21 μm, which was the smallest among all the tested groups, whereas the average hair diameter of the G4 group was 24.43 μm (Fig. 4b). The SEM images revealed that the regenerated hair in the G2-G6 groups was thick, with intact scales, while the regenerated hair in the G1 group was thin, with unhealthy scales (Fig. 4c). The hair pulls tests demonstrated that the regrown hair in the G3-G6 groups could not be easily peeled off by tape, similar to the natural hair of wild-type mice (G0) (Fig. 4d). These results indicate that the synergistic effect of MXD-loaded MNs, VPA and longer electrical stimulation not only promotes the growth of hair but also improves the quality of regenerated hair. We believe that the main reason for this phenomenon is that electrical stimulation can enhance the regrowth of HF cells by accelerating the telogen-to-anaagen transition. Skin pigmentation occurs because of the for-

mation of melanin by HFs during the transition from the resting to anagen state. This hypothesis was confirmed by H&E images of hair-regenerated skin tissue after 20 days of administration, as shown in Fig. 4e. Only a small number of HF cells were observed in the G1 group. However, a large number of HF cells were found in the G2-G6 groups after electrical stimulation. In particular, in the case of the G4 group, the most active HF cells were obtained, indicating an earlier transition into the anagen phase in all groups.

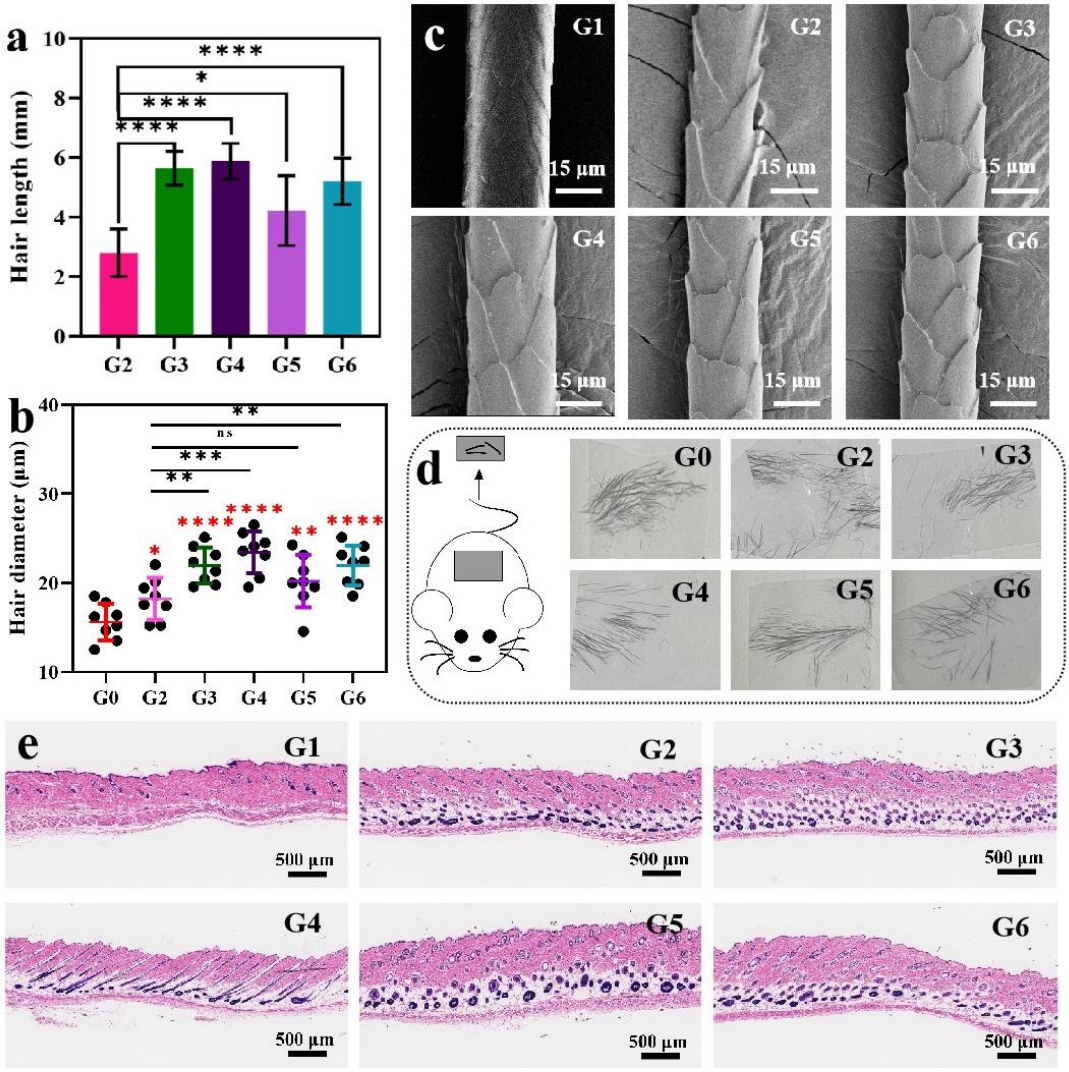

Figure 4 Comparison of hair length (a) and hair diameter (b) after administration for 20 days, SEM images of regrowth hair in G1-G6 (c), hair pull tests of regrowth hair by the tape assay in G2-G6 groups in comparison with the wild-type mice (G0) as a control (d), H&E staining images of hair regenerated skin tissue after 20 days administration (e).

The epidermal thicknesses were also tested after 12 days of administration (Fig. 5a). Among them, the G4 and G0 groups exhibited no significant differences in epidermal thickness. These findings indicated that MXD-loaded MNs, VPA, and positive electrical stimulation promoted hair regeneration without irreversible damage to the skin. High expression of the inflammatory factor interleukin-6 (IL-6) inhibits the growth and proliferation of dermal papilla cells (DPCs), which inhibits hair growth [10, 51]. Fig. 5b shows that the highest secretion levels of IL-6 were observed in the G5 and G6 groups, while there was a slight decrease in IL-

6 in the G3 and G4 groups after 20 days of administration. In addition to mechanical insertion, MXD-loaded MNs may contribute to the emergency response to inflammation caused by negative electrical stimulation. However, a significant decrease in IL-6 expression can be obtained after electrical stimulation, indicating that it can suppress the secretion of IL-6 and reduce the risk of inflammation. Fig. 5c shows images of IL-6-stained hair-regenerated skin tissue after 20 days of treatment. The G4 group exhibited the lowest amount of IL-6 staining, which is consistent with the decrease in IL-6 secretion.

The expression of vascular endothelial growth factor (VEGF) affects the apoptosis of hair follicle stem cells [7]. Fig. 5d shows VEGF staining images of hair-regenerated skin tissue after 20 days of administration. The highest level of VEGF was observed in the G4 group (Fig. 5e), showing the synergistic effect of MXD-loaded MNs, VPA, and positive electrical stimulation on accelerating VEGF secretion in the alopecia area. However, lower levels of VEGF can be observed after the incorporation of negative electrical stimulation into MXD-loaded MNs and VPA. Based on the above results, in MXD-loaded MNs, VPA and electrical stimulation for 60 min exhibit anti-inflammatory activity and hair growth-promoting effects and have potential applications in the treatment of androgenetic alopecia.

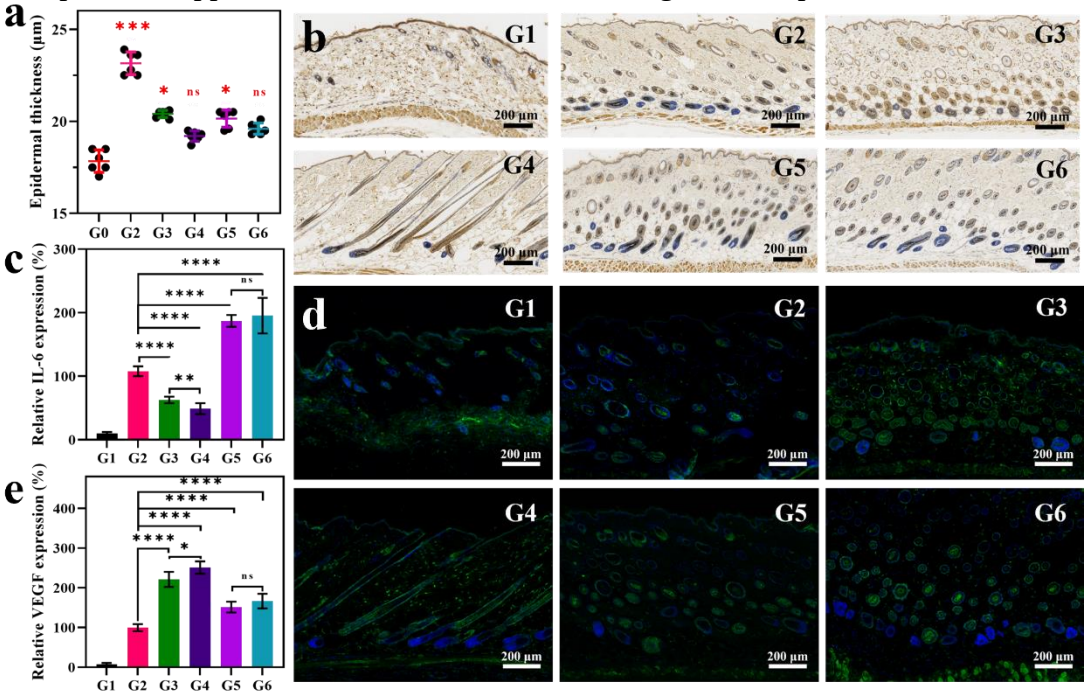

Figure 5 Epidermal thickness after administration for 20 days (a), IL-6 staining images of the G1-G6 groups after administration for 20 days (b), quantitative analysis results of IL-6 staining (c), VEGF staining images of the G1-G6 groups after administration for 20 days (d) and quantitative analysis results of VEGF staining in the G1-G6 groups (e).

In vivo inflammatory factor and VEGF expression can be used to estimate hair regeneration efficacy. First, a nude mouse (BALBc nude) model was established. As shown in Fig. 6a, different administration strategies were used on days 3, 9 and 15. No hair developed within 20 days in G7 (control group: without electrical stimulation) due to immunodeficiency and low levels of VEGF. The HF cells begin the anagen phase after 10 days, and the hair begins to grow (Fig. 6b). The effects of MXD-loaded MNs, VPA, and electrical stimulation for 60 min on hair regrowth were further evaluated by quantifying the hair coverage area (cm^2), length

(mm), diameter (μm) and hair density (shafts/cm^2) over the dorsal skin area, as shown in Table S3. During the entire treatment, the nude mice in the control group (G7) were in the quiescent phase and exhibited almost no hair regrowth (31±2 shafts/cm^2). However, a noticeable synergistic effect on hair regeneration was also observed in the G8 group with positive electrical stimulation. An accelerated transition was observed in the G8 group due to the increased expression of VEGF. Only a very small and unhealthy amount of HF cells and lower levels of IL-6 and VEGF secretion were observed in the G7 group (Fig. 6c). In addition, more healthy HF cells, more inflammatory cells with a greater level of IL-6 secretion and greater expression of VEGF can be found with the synergistic treatment of MXD-loaded MNs, VPA and positive electrical stimulation (Fig. 6d).

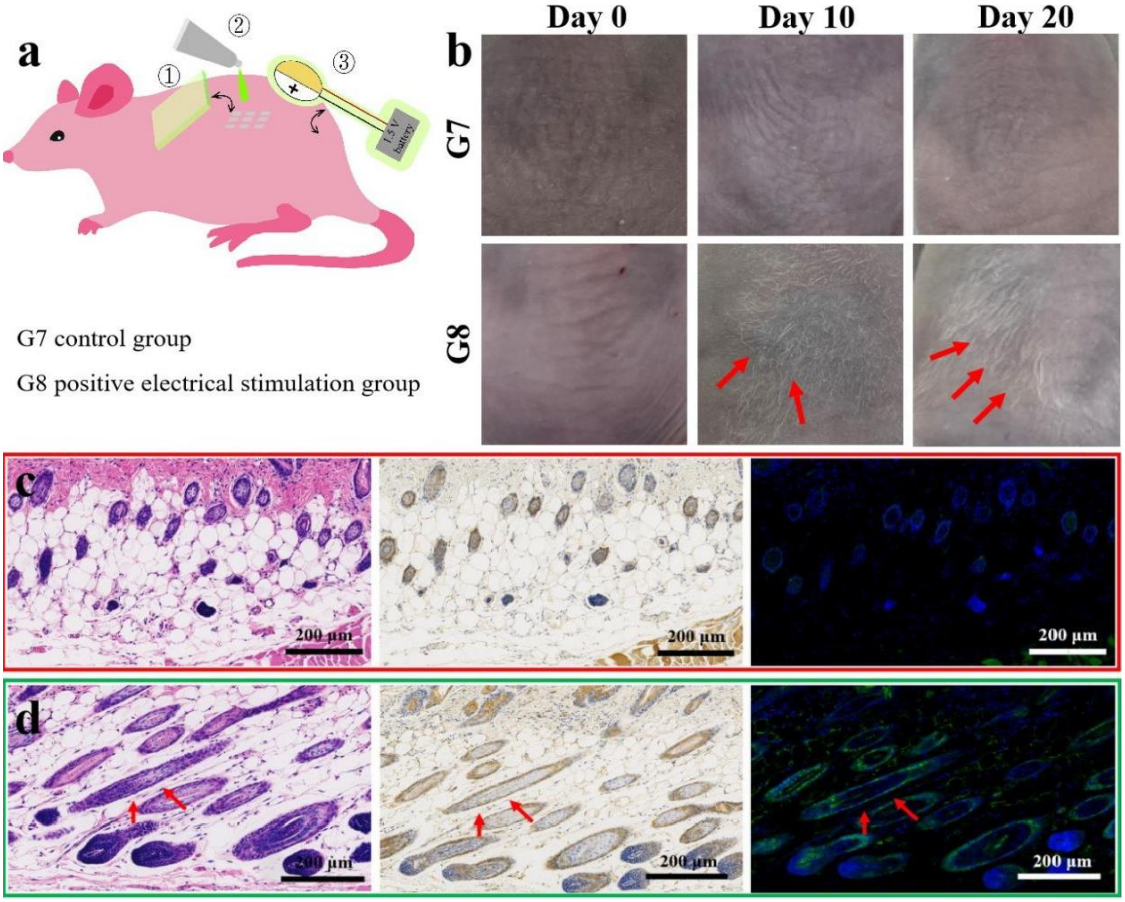

Figure 6 Schematic representation of the establishment and therapeutic strategies of the nude mice (a), representative images of the G7 and G8 groups after administration for 0, 10 and 20 days (b), H&E staining, IL-6 staining, and VEGF staining images of the G7 group (c) and G8 group (d) after administration for 20 days.

4. Conclusion

In this study, an MXD-loaded MN system with the assistance of VPA was developed to treat AGA under electrical stimulation (ES). *In vivo* assays revealed that in clinical AGA treatment, the diffusion of MXD and VPA into skin tissue can be accelerated through microchannels produced by MNs, thereby promoting cell proliferation, accelerating hair follicle renewal, and facilitating hair follicle recovery. Moreover, electrical stimulation can achieve greater hair regeneration coverage in the AGA mouse model in combination with MXD-loaded MNs and VPA than without electrical stimulation, even with decreased electrical stimulation frequency. In addition, the synergistic effect of MXD-loaded microneedles, VPA, and

positive electrical stimulation could boost perifollicular vascularization, activate hair follicle stem cells, decrease inflammation effectively, and promote VEGF, showing potential application in the treatment of AGA.

Conflicts of Competing Interest

The authors declare that they have no known competing business interests or personal relationships that could have appeared to influence the work reported in this paper.

Data availability

The data will be made available upon request.

Acknowledgments

This research was supported by the Huadong Medicine Joint Funds of the Zhejiang Provincial Natural Science Foundation of China under Grant No. LHDMZ23H300003 and the National Natural Science Foundation of China under Grant No. 51873194 and "Scientific and Practical Foundations for the Development of Original Drugs and Biomaterials Containing Nanostructured and Biologically Active Metal Nanoparticles on the base Natural Biodegradable Polymers and Their Derivatives" Scientific Research Program of the Academy of Sciences of the Republic of Uzbekistan for 2025.

REFERENCES

[1] A.T. Talebzadeh, N. Talebzadeh, Stem cell applications in human hair growth: a literature review, Cureus J. Med. Sci. 15 (2023) 37439.

[2] Y. Gu, Q. Bian, Y. Zhou, Q. Huang, J. Gao, Hair follicle-targeting drug delivery strategies for the management of hair follicle-associated disorders, Asian J. Pharm. Sci. 17 (2022) 333-352.

[3] A. G. Evans, J. M. Mwangi, R. W. Pope, M. G. Ivanic, M. A. Botros, G. E. Glassman, F. B. Pearce, Jr., S. Kassis, Platelet-rich plasma as a therapy for androgenic alopecia: a systematic review and meta-analysis, J. Dermatol. Treat. 33 (2022) 498-511.

[4] S. Paul, I. Licona-Vazquez, F. I. Serrano-Cano, N. Frias-Reid, C. Pacheco-Dorantes, S. Pathak, S. Chakraborty, A. Srivastava, Current insight into the functions of microRNAs in common human hair loss disorders: a mini review, Hum Cell 34 (2021) 1040-1050.

[5] J. Griggs, B. Burroway, A. Tosti, Pediatric androgenetic alopecia: a review, J. Am. Acad. Dermatol. 85 (2021) 1267-1273.

[6] M. Zhu, D. Kong, R. Tian, M. Pang, M. Mo, Y. Chen, G. Yang, H. Cheng, X. Lei, K. Fang, B. Cheng, Y. Wu, Platelet sonicates activate hair follicle stem cells and mediate enhanced hair follicle regeneration, J. Cell. Mol. Med. 24 (2020) 1786-1794.

[7] X. Zhang, D. Zhou, T. Ma, Q. Liu, Vascular endothelial growth factor protects CD200-rich and CD34-positive hair follicle stem cells against androgen-induced apoptosis through the phosphoinositide 3-Kinase/Akt pathway in patients with androgenic alopecia, Dermatol. Surg. 46 (2020) 358-368.

[8] C. C. Zouboulis, K. Degitz, Androgen action on human skin -- from basic research to clinical significance, Exp. Dermatol. 13 (2004) 5-10.

[9] W. Zheng, F. Wang, N. Tao, X. Wang, X. Jin, C. Zhang, C. Xu, An androgenetic alopecia remedy based on marine collagen peptide-incorporated dissolving microneedles, Int. J. Pharm. 650 (2024) 123629.

[10] J. Xiong, Z. Liu, L. Jia, Y. Sun, R. Guo, T. Xi, Z. Li, M. Wu, H. Jiang, Y. Li, Bioinspired engineering ADSC nanovesicles thermosensitive hydrogel enhance autophagy of dermal papilla cells for androgenetic alopecia treatment, Bioact. Mater. 36 (2024) 112-125.

[11] Z. Liu, Z. He, X. Ai, T. Guo, N. Feng, Cardamonin-loaded liposomal formulation for improving percutaneous penetration and follicular delivery for androgenetic alopecia, Drug Deliv. Transl. Res. (2024) doi: 10.1007/s13346-024-01519-8.

[12] B. Roets, Potential application of PBM use in hair follicle organoid culture for the treatment of androgenic alopecia, Mater. Today Bio. 23 (2023) 100851.

[13] G. Yang, G. Chen, Z. Gu, Transdermal drug delivery for hair regrowth, Mol. Pharm. 18 (2021) 483-490.

[14] S. Watanabe, Y. Kuwabara, S. Suehiro, D. Yamashita, M. Tanaka, A. Tanaka, S. Ohue, H. Araki, Valproic acid reduces hair loss and improves survival in patients receiving temozolomide-based radiation therapy for high-grade glioma, Eur. J. Clin. Pharmacol. 73 (2017) 357-363.
[15] E. Kalabusheva, V. Terskikh, E. Vorotelyak, Hair germ model *in vitro* via human postnatal keratinocyte-dermal papilla interactions: impact of hyaluronic acid, Stem Cells Int. 2017 (2017) 9271869.
[16] D. Liu, Q. Xu, X. Meng, X. Liu, J. Liu, Status of research on the development and regeneration of hair follicles, Int. J. Med. Sci. 21 (2024) 80-94.
[17] T. Xiao, B. Li, R. Lai, Z. Liu, S. Xiong, X. Li, Y. Zeng, S. Jiao, Y. Tang, Y. Lu, Y. Xu, Active pharmaceutical ingredient-ionic liquids assisted follicular codelivery of ferulic acid and finasteride for enhancing targeted anti-alopecia, Int. J. Pharm. 648 (2023) 123624.
[18] F. F. V. Santana, A. A. Lozi, R. V. Goncalves, J. Da Silva, S. L. P. Da Matta, Comparative effects of finasteride and minoxidil on the male reproductive organs: a systematic review of *in vitro* and *in vivo* evidence, Toxicol. Appl. Pharmacol. 478 (2023) 116710.
[19] M. J. Bertoli, R. Sadoughifar, R. A. Schwartz, T.M. Lotti, C. K. Janniger, Female pattern hair loss: a comprehensive review, Dermatol. Ther. 33 (2020) e14055.
[20] J. H. Upton, R. F. Hannen, A. W. Bahta, N. Farjo, B. Farjo, M. P. Philpott, Oxidative stress-associated senescence in dermal papilla cells of men with androgenetic alopecia, J. Invest. Dermatol. 135 (2015) 1244-1252.
[21] A. N. Sharma, L. Michelle, M. Juhasz, P. Muller Ramos, N. Atanaskova Mesinkovska, Low-dose oral minoxidil as treatment for nonscarring alopecia: a systematic review, Int. J. Dermatol. 59 (2020) 1013-1019.
[22] H. Xing, H. Peng, Y. Yang, K. Lv, S. Zhou, X. Pan, J. Wang, Y. Hu, G. Li, D. Ma, Nitric oxide synergizes minoxidil delivered by transdermal hyaluronic acid liposomes for multimodal androgenetic-alopecia therapy, Bioact. Mater. 32 (2024) 190-205.
[23] D. Song, S. Pan, W. Jin, R. Wu, T. Zhao, J. Jiang, M. Zhu, Minoxidil delivered via a stem cell membrane delivery controlled release system promotes hair growth in C57BL/6J mice, Front. Bioeng. Biotech. 11 (2024) 1331754.
[24] P. Gentile, S. Garcovich, Systematic review of platelet-rich plasma use in androgenetic alopecia compared with minoxidil, finasteride, and adult stem cell-based therapy, Int. J. Mol. Sci. 21 (2020) 2702.
[25] Y. Shen, Y. Zhu, L. Zhang, J. Sun, B. Xie, H. Zhang, X. Song, New target for minoxidil in the treatment of androgenetic alopecia, Drug Des. Dev. Ther. 17 (2023) 2537-2547.
[26] A. Makhlouf, T. Elnawawy, Hair regrowth boosting via minoxidil cubosomes: formulation development, *in vivo* hair regrowth evaluation, histopathological examination and confocal laser microscopy imaging, Int. J. Pharm. 634 (2023) 122665.
[27] S. F. Lahiji, S. H. Seo, S. Kim, M. Dangol, J. Shim, C. G. Li, Y. Ma, C. Lee, G. Kang, H. Yang, K.-Y. Choi, H. Jung. Transcutaneous implantation of valproic acid-encapsulated dissolving microneedles induces hair regrowth. Biomaterials, 167 (2018) 69-79.
[28] G. Shamloul, A. Khachemoune, An updated review of the sebaceous gland and its role in health and diseases part 2: pathophysiological clinical disorders of sebaceous glands, Dermatol. Ther. 34 (2021) e14862.
[29] M. Roohaninasab, A. Goodarzi, M. Ghassemi, A. Sadeghzadeh-Bazargan, E. Behrangi, N. Najar Nobari, Systematic review of platelet-rich plasma in treating alopecia: focusing on efficacy, safety, and therapeutic durability, Dermatol. Ther. 34 (2021) 2702.
[30] D. Pei, L. Zeng, X. Huang, B. Wang, L. Liu, G. Zhang, Efficacy and safety of combined microneedling therapy for androgenic alopecia: a systematic review and meta-analysis of randomized clinical trials, J. Cosmet. Dermatol. 23 (2024) 1560-1572.
[31] Y. Zhou, L. Jia, D. Zhou, G. Chen, Q. Fu, N. Li, Advances in microneedles research based on promoting hair regrowth, J. Control Release 353 (2023) 965-974.
[32] R. Wang, G. Jiang, U. E. Aharodnikau, K. Yunusov, Y. Sun, T. Liu, S.O. Solomevich, Recent advances in polymer microneedles for drug transdermal delivery: design strategies and applications, Macromol. Rapid Commun. 43 (2022) 2270022.
[33] S. Ruan, Y. Zhang, N. Feng, Microneedle-mediated transdermal nanodelivery systems: a review, Biomater. Sci. 9 (2021) 8065-8089.
[34] S. Duarah, M. Sharma, J. Wen, Recent advances in microneedle-based drug delivery: special emphasis on its use in pediatric population, Eur. J. Pharm. Biopharm. 136 (2019) 48-69.

[35] L. Yan, T. Kageyama, B. Zhang, S. Yamashita, P. J. Molino, G. G. Wallace, J. Fukuda, Electrical stimulation to human dermal papilla cells for hair regenerative medicine, J. Biosci. Bioeng. 133 (2022) 281-290.
[36] D. M. Sondagar, H. H. Mehta, R. S. Agharia, M. K. Jhavar, Efficacy of low-level laser therapy in androgenetic alopecia - a randomized controlled trial, Int. J. Trichol. 15 (2023) 25-32.
[37] G.E. Glass, Photobiomodulation: The clinical applications of low-level light therapy, Aesthet. Surg. J. 41 (2021) 723-738.
[38] H. Galadari, S. Shivakumar, T. Lotti, U. Wollina, A. Goren, G. R. Rokni, S. Grabbe, M. Goldust, Low-level laser therapy and narrative review of other treatment modalities in androgenetic alopecia, Lasers Med. Sci. 35 (2020) 1239-1244.
[39] D. Heo, S. Jung, J. Kim, H. Yong, S. Park, D. Kim, S. Cho, K. Cha, H. Ryu, Y. Jin, W. Lee, S. Lee, J. Hong, Human activity-driven self-powered hair follicle stimulation system, Nano Energy 103 (2022) 107772.
[40] B. Benjamin, D. Ziginskas, J. Harman, T. Meakin, Pulsed electrostatic fields (ETG) to reduce hair loss in women undergoing chemotherapy for breast carcinoma: a pilot study, Psychooncology 11 (2002) 244-248.
[41] D. Hwang, H. Lee, J. Lee, M. Lee, S. Cho, T. Kim, H. Kim, Microcurrent stimulation has potential effects of hair growth-promotion on human hair follicle-derived papilla cells and animal model, Int. J. Mol. Sci. 22 (2021) 4361.
[42] G. Yao, D. Jiang, J. Li, L. Kang, S. Chen, Y. Long, Y. Wang, P. Huang, Y. Lin, W. Cai, X. Wang, Self-activated electrical stimulation for effective hair regeneration via a wearable omnidirectional pulse generator, ACS Nano 13 (2019) 12345-12356.
[43] K. M. Sohn, K. H. Jeong, J.E. Kim, Y. M. Park, H. Kang, Hair growth-promotion effects of different alternating current parameter settings are mediated by the activation of Wnt/β-catenin and MAPK pathway, Exp. Dermatol. 24 (2015) 958-963.
[44] H. Xiang, S. Xu, W. Zhang, X. Xue, Y. Li, Y. Lv, J. Chen, X. Miao, Dissolving microneedles for alopecia treatment, Colloid. Surface. B. 229 (2023) 113475.
[45] A. J. Paredes, F. Volpe-Zanutto, A. D. Permana, A.J. Murphy, C. J. Picco, L.K. Vora, J. A. Coulter, R.F. Donnelly, Novel tip-loaded dissolving and implantable microneedle array patches for sustained release of finasteride, Int. J. Pharm. 606 (2021) 120885.
[46] A. A. Elshall, A. M. Ghoneim, N. M. Abd-elmonsif, R. Osman, D. S. Shaker, Boosting hair growth through follicular delivery of melatonin through lecithin-enhanced pickering emulsion stabilized by chitosan-dextran nanoparticles in testosterone induced androgenic alopecia rat model, Int. J. Pharm. 639 (2023) 122972.
[47] R. Wang, H. Wang, G. Jiang, Y.F. Sun, T. Liu, L. Nie, A. Shavandi, K. E. Yunusov, U. E. Aharodnikau, S. O. Solomevich, Transdermal delivery of allopurinol to acute hyperuricemic mice via polymer microneedles for the regulation of serum uric acid levels, Biomater. Sci. 11 (2023) 1704-1713.
[48] K. Prabahar, U. Uthumansha, N. Elsherbiny, M. Qushawy, Enhanced skin permeation and controlled release of β-sitosterol using cubosomes encrusted with dissolving microneedles for the management of alopecia, 16 (2023) 563.
[49] T. Liu, Y. Sun, G. Jiang, W. Zhang, R. Wang, L. Nie, A. Shavandi, K.E. Yunusov, U.E. Aharodnikau, S.O. Solomevich, Porcupine-inspired microneedles coupled with an adhesive back patching as dressing for accelerating diabetic wound healing, Acta Biomater. 160 (2023) 32-44.
[50] J.-S. Ong, M. Seviiri, J.C. Dusingize, Y. Wu, X. Han, J. Shi, C.M. Olsen, R.E. Neale, J.F. Thompson, R.P.M. Saw, K.F. Shannon, G.J. Mann, N.G. Martin, S.E. Medland, S.D. Gordon, R.A. Scolyer, G.V. Long, M.M. Iles, M.T. Landi, D.C. Whiteman, S. Macgregor, M.H. Law, Uncovering the complex relationship between balding, testosterone and skin cancers in men, Nat. Commun. 14 (2023) 5962.
[51] M.H. Kwack, C.H. Seo, P. Gangadaran, B.-C. Ahn, M.K. Kim, J.C. Kim, Y.K. Sung, Exosomes derived from human dermal papilla cells promote hair growth in cultured human hair follicles and augment the hair-inductive capacity of cultured dermal papilla spheres, Exp. Dermatol. 28 (2019) 854-857.